Published in final edited form as:
Neuroimage. 2012 January 2; 59(1): . doi:10.1016/j.neuroimage.2011.07.067.

Relationship between aberrant brain connectivity and clinical features in Angelman Syndrome: a new method using tract based spatial statistics of DTI color-coded orientation maps

Vijay N. Tiwari, MD PhD[1,2], **Jeong-won Jeong, PhD**[1,2], **Benjamin J. Wilson, BA**[1,2], **Michael E Behen, PhD**[1,2], **Harry T. Chugani, M.D**[1,2], and **Senthil K. Sundaram, M.D.**[1,2]

[1]Departments of Pediatrics and Neurology Children's Hospital of Michigan, Wayne State University, Detroit, MI

[2]PET Center, Children's Hospital of Michigan, Detroit Medical Center, Detroit, MI

Abstract

Aim—In order to relate brain structural abnormalities to clinical features of Angelman Syndrome (AS), we determined the locations of abnormal regional white matter architecture in AS children using a sensitive and objective whole brain approach to analyze diffusion tensor imaging (DTI) color-coded orientation maps.

Methods—Using tract based spatial statistics (TBSS) of DTI color-coded orientation maps, the fraction of fibers oriented in the anteroposterior (AP), mediolateral (ML) and superioinferior (SI) directions were determined in whole brain white matter of 7 children with AS (mean age: 70 ± 25.78 months, 5 males) and 7 children with typical development (TD, mean age: 79.8 ± 17.25 months, 4 males). TBSS of FA map was also performed for comparison.

Results—Children with AS had a significantly lower AP component than the TD group in 9 clusters (3 bilateral and 3 unilateral). Bilateral clusters were located in inferior fronto-occipital fasciculus, anterior thalamic radiation and arcuate fasciculus regions. Unilateral clusters involved left brainstem, left cingulum and right uncinate regions. Similarly, children with AS had significantly lower ML component than the TD group in 4 clusters (2 in corpus callosum and 2 unilateral clusters). Unilateral clusters were located in the left cingulum and left anterior thalamic radiation regions. SI component was lower in children with AS in two clusters compared to TD (corticospinal tract and corpus callosum). FA map clusters mostly corresponded with component clusters.

Interpretation—Children with AS have a global impairment of white matter integrity including AP, ML and SI components in whole brain suggesting a potential underlying error with axon guidance mechanisms during brain development possibly due to loss of UBE3A gene expression. Some of this aberrant connectivity can be related to the clinical features of AS.

Keywords

Angelman Syndrome; DTI; Color-coded TBSS

Address for Correspondence: Senthil K. Sundaram, M.D. Children's Hospital of Michigan PET Center 3901 Beaubien Blvd. Detroit MI 48201. Telephone: (313) 993-2870 Fax: (313) 966-9228 ssundaram@pet.wayne.edu.

Introduction

Angelman syndrome (AS) is a neurogenetic disorder characterized by developmental delay, severe intellectual disability, absent speech, exuberant behavior with happy demeanor, motor impairment and epilepsy, due to deficient *UBE3A* gene expression that may be caused by various abnormalities of chromosome 15 (Dan, 2009). There are several genetic mechanisms related to AS: de novo deletions of maternal 15q11-13, uniparental paternal disomy of 15q11-13, imprinting defect, or mutation of the UBE3A gene (Clayton-Smith and Laan, 2003). Each of these mechanisms includes a loss in expression of the UBE3A gene.

Despite the severe neurodevelopmental phenotype of AS, brain magnetic resonance imaging (MRI) typically reveals normal findings. In an effort to relate brain anatomy to clinical phenotype in AS, our group(Wilson BJ et al, 2010; Wilson BJ et al., 2011)and subsequently others(Peters et al., 2011) have studied the major brain tracts using diffusion tensor imaging (DTI) with tractography and have shown very consistent abnormalities in various cortical association tracts, including the arcuate fasciculus thus accounting for the virtual absence of speech in these individuals.

DTI assesses the diffusion pattern of water molecules in order to provide information about white matter tracts and/or tissue architecture. Given the individual differences in brain size, shape and orientation, objective and unbiased analysis methods are preferable to the manual methods such as tractography used in previous studies. A recently developed more objective analysis method is tract based spatial statistics (TBSS). TBSS is a sensitive, operator independent and accurate voxel based white matter analysis method for multi-subject diffusion imaging studies(Smith et al., 2006). Indeed, TBSS has been used successfully to evaluate white matter integrity, particularly fractional anisotropy (FA) measurements, in a wide variety of neurological and psychiatric conditions such as Alzheimer's disease(Stricker et al., 2009), multiple sclerosis(Roosendaal et al., 2009), bipolar disorder(Versace et al., 2008), substance abuse(Choi et al., 2009) and autism spectrum disorder(Cheng et al., 2010). Typically FA and apparent diffusion coefficient (ADC) maps are used in TBSS analysis. Given that these are scalar measures, crucial *orientation* information is lost in this process. Although DTI tractography can provide orientation information by reconstruction of the tracts, aberrant connectivity cannot be easily quantified by this approach. In addition, one has to define *a priori* regions of interest (ROIs) in tractography to isolate individual tracts, but these ROIs can be defined reasonably well only for large tracts. Moreover, outside of some major tracts, the process can be highly subjective. Thus, a method that combines the objectivity of TBSS with the orientation information of tractography is highly desirable. In the present study, we have performed TBSS on DTI color-coded orientation maps (instead of FA/ADC maps) to maximize the advantages of both methods in a population of AS and typically developing (TD) children. A second goal of this study was to relate the aberrant brain connectivity to the main clinical features. Furthermore, we also compared TBSS performed in DTI color-coded orientation maps with TBSS using FA maps in the same population.

Methods

Participants

Seven AS participants (age: 70 ± 25.78 months, five males) and seven age-matched typically developing (TD) children (age: 79.8 ± 17.25 months, four males) were studied. TD participants had measured intellectual functioning within one standard deviation of the normative mean, and none had any current or historical medical or psychiatric diagnoses. AS participants underwent fluorescent in situ hybridization (FISH) or methylation testing to confirm their diagnosis. In the AS group, five subjects had deletions in the 15q11-13

genomic region. One participant had confirmed uniparental paternal disomy (UPD) and one participant presented with abnormal small nuclear ribonuleoprotein polypeptide N (SNRPN) methylation testing, but additional information regarding the specific genetic lesion was not available. Five out of the seven AS participants were recruited for this study and written informed consent was obtained from one of the parents or legal guardians. Data from the remaining two of the seven AS participants were obtained clinically. The Human Investigations Committee (HIC) of Wayne State University and Institutional Review Board of Detroit Medical Center (Children's Hospital of Michigan is part of Detroit Medical Center) granted permission for the retrieval and analysis of archived clinical data. The study was approved by the Institutional Review Board at Wayne State University and Detroit Medical Center.

The TD group was part of a separate normal controls study. They were administered portions of either the Wechsler Intelligence Scale for children-Third Edition or the Wechsler Preschool Primary scale of Intelligence-Third Edition (Wechsler, 2002; Wechsler 2003). The version of the test administered depends on the age of the child (WPPSI-III for ages 4:0-5:9; WISC-III for age 6:0-16:0). One child, a non-english speaking child completed the Colored Progressive Matrices Test (CPM, Raven, Court & Raven, 1990), a measure of nonverbal intellectual functioning. The CPM is widely used measure of nonverbal intellectual functioning and has been demonstrated to have adequate psychometric properties (Sattler, 1992). All controls had measured IQs above 85.

All children included in the TD group had: (a) measured intellectual functioning within normal limits (≥85); (b) normal neurological screening; and (c) absence of any current or historical medical or psychiatric diagnoses, (d) not taking any regular medications, (e) no clinical elevations on a caregiver-reported measure of behavioral problems (BASC). In addition children with any of the following were also specifically excluded from this study: (a) history of seizures, (b) focal deficits on clinical examination by a pediatric neurologist, (c) MRI finding interpreted as abnormal by a pediatric neuroradiologist, (d) dysmorphic features suggestive of a genetic abnormality (including fragile X syndrome), (e) an inborn error of metabolism, and (f) history of prematurity or perinatal hypoxic-ischemic event.

Five out of the seven AS participants completed developmental evaluations assessing global cognitive functioning, fine motor skills, language functioning, parent ratings of adaptive behavior and caregiver report of behavioral functioning. Vineland Adaptive Behavior Scales-II was used to perform neuropsychological examination [Vineland Adaptive Behavior Scales, 2nd edition (VABS, Sparrow et al. 1984)].

DTI Acquisition protocol

MRI scans were performed with a 3 Tesla Twin-Speed GE Scanner using an 8-channel head coil. The MRI acquisition consisted of spin-echo echo-planar diffusion weighted sequence acquired in axial plane with 55 diffusion sensitization gradients (b = 1000 [s/mm2]) applied in non-collinear directions (Di, i = [1, … , 55]) and a T2-weighted reference (D0) scan (b = 0 [s/mm^2]). The diffusion weighted sequence consisted of the following imaging parameters: a set of minimum 34 axial slices of 3-mm thickness without gap, field of view = 240 × 240 mm^2, matrix = 128 × 128 reconstructed with homodyne to 256 × 256, repetition time/echo time = 9000 to 11000/80 milliseconds. Double radio frequency refocusing pulses and parallel imaging capability (ASSET factor of 2) were applied to reduce eddy current and geometric distortion artifacts derived from echo-planar imaging. Because the scans for AS participants were clinical MRI studies, sedation was used as necessary by the sedation team at Children's Hospital of Michigan according to standard clinical protocols. None of the TD children were sedated for the MRI. However, younger children were scanned while sleeping,

and all children were monitored for movement during scan. If there was significant movement, MRI was repeated or those scans were removed from the study.

DTI color-coded orientation maps

The direction of individual fibers in diffusion tensor imaging data can be imaged by color-coded orientation maps, where three components of the eigenvector v_1, in association with the largest eigenvalue, are color coded using a red-green-blue (RGB) color model which is symmetrical with respect to all color axes. The color axes are aligned with the patient coordinate system (green: anterior-to-posterior, red: medial-to-lateral, blue: superior-to-inferior). This convention was used as a direct metric to quantify the proportion of fibers in anterior-posterior (AP), medial-lateral (ML) and superior-inferior (SI) components. The direction of individual fibers in diffusion tensor imaging data can be imaged by color encoded orientation maps, where three components of the eigenvector v 1 , in association with the largest eigen value, are color coded using an RGB-color model which is symmetrical with respect to all color axes. This is given by the equation (r, g, b) = FA · (v x , v y , v z) (Jiang et al., 2006) where *r, g,* and *b* represent red, green, and blue components of the voxel color, and (v *x* , v y , v z) is the normalized principal eigenvector.

Tensor calculation and TBSS analysis of color coded orientation maps

The entire DT-MRI image data set was visually inspected and affine corrected for motion and other imaging artifacts; Correction for eddy induced distortions was performed using a mutual information-based registration of all images to the mean non-diffusion-weighted images. Six diffusion tensor element images of individual participant were generated using an in-house implemented software incorporating a signal-to-noise-ratio weighed multivariate least square fitting approach (Basser and Pierpaoli et al., 1996) and spatially normalized into the MNI space where the tensor field was properly reoriented according to local deformation (Alexander et al., 2001; Xu et al., 2003). The reoriented tensor images were finally utilized to produce the maps of FA, AP, ML and SI in MNI space using conventional prinicpal component analysis of diffusion tensor matrix (Brun A et al., 2003).

TBSS (Smith et al., 2006) was conducted using the MNI FA, AP, ML and SI maps of individual participants. The initial step of TBSS analysis consisted of voxel-wise nonlinear registration of all participant's FA images to a target image which is a predetermined pediatric FA template in MNI space. The obtained nonlinear transformation was also applied for the AP, ML and SI images of corresponding participant. The transformed FA, AP, ML and SI images of all participants were averaged to create mean images. The mean FA image was then used to create a skeleton image of the white matter tracts using a protocol which searches and labels the skeleton voxels with maximum FA, AP, ML and SI component values along the perpendicular direction (breath) of a white matter tract. The mean skeleton, derived from the mean FA image, was identified at the exact median of the white matter tract. This mean skeleton was later applied to the registered FA, AP, ML and SI component images of individual participants. FA map images were used for the coregistration/ normalization steps of TBSS and then AP, ML and SI maps were used for statistical comparisons. Following the search for the maximum AP ML and SI component value along the width of the white matter tract, perpendicular to the skeleton voxel, the maximum AP ML and SI component values were then projected onto the skeleton voxel for further statistical analysis. These skeletonised green and red component images were now subjected to voxelwise cross-subject analysis using the randomization toolbox in FSL.

Voxel-wise cross-subject statistical analysis was performed using individual skeleton images of the TD group compared to each of the AS groups for both contrasts (TD > AS, TD > AS) with age as a covariate, using nonparametric permutation tests (5000 permutations/design),

with a cluster size threshold of >3 and a p value of <0.05 for significance, after correcting for multiple comparisons. The p<0.05 significance threshold was used due to the multiple design matrices, to avoid false positive results. Skeletal voxels, which were significantly different between the groups, were isolated, labeled and expanded to include the full width of the white matter tract, which was then used as a mask permitting calculation of the mean AP, ML and SIcomponent values for the width of the tract for individual participants. Although, showing the results on the TBSS skeleton is a true representation of the actual analysis, it is easier to visualize the results if the skeletonised results are "thickened' further using a filling process. We determined the most probable anatomic localization of each cluster by means of the FSL atlas tool (http://www.fmrib.ox.ac.uk/fsl/data/atlas-descriptions.html/), which incorporates several anatomic templates, including the Talaraich atlas, MNI structural atlas, Julich histological atlas, Oxford thalamic connectivity atlas, Harvard-Oxford atlas, sub-cortical structural atlases and the John Hopkins University DT-MRI based white matter atlases.

Tensor calculation and TBSS analysis of FA maps

After generating FA images for all the participants as described previously, the initial step of TBSS analysis consisted of voxel-wise nonlinear registration of all participants to a target image provided by the FSL software. The transformed FA images of all participants were averaged to create a mean FA image. This mean FA image was then used to create a skeleton image of the white matter tracts using a protocol which searches and labels the skeleton voxels with maximum FA intensity along the perpendicular direction (breath) of a white matter tract. An FA threshold of 0.2 was used to differentiate between grey and white matter. The mean skeleton, derived from the mean FA image, was identified at the exact median of the white matter tract. This mean skeleton was later applied to the registered FA image of individual participants. Following the search for the maximum FA value along the width of the white matter tract, perpendicular to the skeleton voxel, the maximum FA values were then projected onto the skeleton voxel for further statistical analysis. These skeletonised FA images were now subjected to voxelwise cross-subject analysis using the randomization toolbox in FSL.

Voxelwise cross-subject statistical analysis was performed using individual skeleton images of the TD group compared to each of the AS groups for both contrasts (TD > AS) and (TD < AS), with age as a covariate, using nonparametric permutation tests (5000 permutations/design), with a cluster size threshold of >3 and a p value of <0.05 for significance, after correcting for multiple comparisons. The p<0.05 significance threshold was used due to the multiple design matrices, to avoid false positive results. Skeletal voxels, which were significantly different between the groups, were isolated, labeled and expanded to include the full width of the white matter tract, which was then used as a mask permitting calculation of the mean FA values for the width of the tract for individual participants.

Statistical Analysis

Two-sample unpaired t-tests were applied to compare the AS and TD groups. A p-value of less than 0.05 (corrected for multiple comparisons) was considered as statistically significant. Percentage differences of mean AP, ML and SI components between AS and TD group were calculated as follows: % difference = [(mean AP/ML/SI component of TD – mean AP/ML/SI component of AS) / (mean AP/ML/SI component of TD + mean AP/ML/SI component of AS)/2]*100.

Results

The developmental characteristics of the AS children are presented in Table 1. As can be seen, the children in this sample are currently measured in the moderate to severely impaired range across domains with a mean adaptive behavior composite measured in the low range, which are more than two standard deviations below the normative mean. The intellectual functioning data for TD group is summarized below:

PIQ- range:110-124; mean:118.2 ± 7.1

VIQ-range: 94-140; mean: 111.4 ± 17.9

TBSS analysis using DTI color coded orientation maps

Children with AS had a significantly lower AP component than the TD group in 9 clusters (3 bilateral and 3 unilateral) (Table 2). Bilateral clusters were located in inferior fronto-occipital fasciculus, anterior thalamic radiation and arcuate fasciculus regions. Unilateral clusters involved left brainstem, left cingulum and right uncinate regions (Figure 1). Similarly, children with AS had significantly lower ML component than the TD group in 4 clusters (2 in corpus callosum and 2 unilateral clusters) (Table 3). Unilateral clusters were located in the left cingulum and left anterior thalamic radiation regions (Figure 1). SI component was significantly lower in children with AS compared to TD group in two clusters (Table 4) which were located in corpus callosum and corticospinal tract (Figure 1). Percentage differences of mean AP, ML and SI component in each cluster between both groups are shown in Tables 2, 3 and 4. The scaled component values in our data set range from 0.05 to 0.37 with a theoretical maximum of 0.5. The common areas where AP and ML components were both reduced are cingulum and ATR. There were no clusters where AP, ML or SI component was increased compared to TD group. Correlations between diffusion tensor imaging metrics (AP, ML and SI components) and Vineland Adaptive Behavior domains were also examined; none of the correlations reached significance. However, a trend towards significance was observed between 5^{th} cluster of AP component (left anterior thalamic radiation) and Vineland socialization score ($p = 0.11$). Additionally, a trend towards significance was also observed between 4^{th} cluster of ML component (right cingulum) and Vineland communication ($p=0.13$); daily living skills ($p=0.14$); socialization scores ($p=0.14$).

TBSS analysis using FA maps

Children with AS had significantly lower FA values than TD in various areas of the brain. These clusters of significantly reduced FA are summarized in Table 5. Figure 1 shows representative images of reduced FA clusters along with AP, ML and SI component clusters for comparison purpose. Although most of the FA clusters corresponded with same regions of brain as seen in component clusters, some of the FA clusters were different from the clusters seen in AP, ML and SI components.

Discussion

We recently reported that quantification of the AP, ML and SI components of DTI color-coded orientation maps can be used to identify subtle abnormalities in the perisylvian region of developmentally delayed children (Jeong et al., 2011)and AS patients (Wilson BJ et al., 2011). However, this ROI based DTI color-coded map quantification method is not appropriate for a whole brain approach. TBSS method utilizing AP, ML and SI components of DTI color-coded orientation maps provides quantification as well as spatial orientation of DTI abnormalities. We found significantly decreased AP, ML and SI components in children with AS in the inferior fronto-occipital fasciculus, cingulum, anterior thalamic

radiation, arcuate fasciculus, brainstem and uncinate fasciculus regions of brain. While several of the abnormalities in white matter microstructure observed in the present study are consistent with previous tractography studies in AS (Wilson BJ et al., 2011; Peters et al., 2011), the present study found *additional* abnormalities in regions such as cingulum, anterior thalamic radiation and brainstem. Moreover, in many regions only one of the components (AP/ML/SI) was involved suggesting a specific nature of the abnormality. Cingulum and anterior thalamic radiation were the only regions where both components (AP and ML) were involved and, incidentally, both areas were not reported in previous DTI tractography studies in AS. The scaled component values in our data set range from 0.05 to 0.37 with a theoretical maximum of 1. A component value of 1 corresponds to maximum fiber orientation along the particular component direction with lower values implying less fiber orientation.

We also compared the FA map cluster analysis with individual AP, ML and SI components cluster analysis. We found that although some of the areas where FA was decreased are same as seen in the color map cluster, there are some differences in the clusters involved in both TBSS analysis. The methods provide complementary information since FA is the tensor shape data involving all the three eigen values while color components denote the orientation information in a given principal eigen values. There are two types of advantages of this approach versus TBSS of FA maps. Firstly, in the heterogeneous regions with multiple crossing fibers, FA map may not detect abnormality in terms of principal fiber orientations. For example in AP cluster number 3 (arcuate region), all three types of fibers (AP, ML and SI) cross in the region, but the abnormality was detected only in AP component. This information cannot be inferred only from FA map. Secondly, even in regions where a single fiber orientation dominates, there is an implicit assumption that the dominant fibers are abnormal whenever FA is low. For example, the white matter through which anterior thalamic radiation passes is typically thought to be homogenous and any FA abnormality is automatically attributed to this tract. However, we found that in this region both AP and ML component are affected leaving only SI component unaffected. This information is obscured in FA map TBSS analysis method.

Previous MRI studies in AS children have revealed delayed myelination, white matter volume reduction and focal white matter signal abnormalities (Castro-Gago et al., 2010; Harting et al., 2009). More specifically, they observed thinning of the corpus callosum, T2 hyper intensities of the periventricular and deep white matter. They also reported reduced myelination of brain white matter. DTI tractography studies on participants with AS have shown abnormalities in arcuate fasciculus, inferior fronto-occipital fasciculus, inferior longitudinal fasciculus, uncinate fasciculus, corticospinal tracts and corpus callosum (Wilson BJ et al., 2011; Peters et al., 2011) and regional abnormalities in almost all of these tracts have been reproduced in the present study.

Anterior thalamic radiation abnormalities in AS: clinical correlations

Seizures are frequently observed in children with AS and distinctive rhythmic EEG patterns are found with good consistency in AS participants (Clayton-Smith and Laan, 2003; Dan and Boyd, 2003)). A number of studies e.g., (Kandel and Buzsaki, 1997) have indicated the central importance of thalamocortical interactions in neuronal firing as a result of synchronization of oscillatory activities between neural populations. Although, these interactions have been studied largely in relation to sleep spindles and childhood absence epilepsy, the EEG patterns in AS bear significant resemblance to that of childhood absence epilepsy (Dan et al., 2004). Furthermore, oscillatory firing in childhood absence epilepsy is known to involve thalamocortical neurons (Hosford et al., 1992; Hosford et al., 1999). In animal models [$GABA_A$ receptor β-subunit 3 deficient mice model] of AS, it has been

shown that this deficiency causes a failure of intrathalamic reticular nucleus inhibition leading to abnormally synchronized thalamocortical oscillations (Handforth et al., 2005). Further evidence in this direction was provided by a ^{11}C-flumazenil PET study in AS patients where decreased flumazenil binding was observed in frontal lobe apart from parietal, hippocampus and cerebellar regions (Holopainen et al., 2001). These multiple lines of evidence suggest involvement of aberrant thalamocortical networks in AS. In this study, we have provided the first objective non-invasive neuroimaging evidence of abnormalities in anterior thalamic radiation region in AS children.

Expressive motor events are normally suppressed by frontal lobe (Kuypers, 1981). Therefore, abnormalities found in the anterior thalamic radiation region in our study could be a reason for the loss of this inhibitory mechanism leading to several symptoms typically observed in AS, such as characteristic laughter and happy puppet demeanor. In fact, patients with frontal lobe damage exhibit little spontaneous facial expression, indicating an important role of frontal lobe in facial expression (Kolb and Milner, 1981).

Arcuate fasciculus abnormalities in AS

Our findings of isolated AP component reduction in bilateral arcuate fasciculus are an objective confirmation of our previous findings of an unidentifiable arcuate fasciculus in AS participants by tractography (Wilson BJ et al., 2011). However, the present study illustrates that by individually analyzing the different components, one can identify the abnormality more specifically. Absence of speech is one of the most striking features of AS and arcuate fasciculus is known to be one of the main pathways for language function. It is interesting to note that while the AP component of arcuate fasciculus region is affected, ML and SI components are not affected. The mechanism of this particular pattern of abnormality is unknown and deserves further investigation.

Cingulum abnormalities in AS

Functional imaging studies have pointed out the role of the anterior cingulum (BA32) and cingulate gyrus (BA24) in the mechanisms underlying theory of mind and empathy (Baron-Cohen, 1991). The anterior cingulum also has a regulatory role between cognitive and emotional processes through its links to hypothalamic-pituitary and brainstem structures (Mayberg, 1997). Additionally, the cingulate network is involved in the initiation and maintenance of motivation to complete an action (Koechlin and Summerfield, 2007). Involvement of anterior cingulum and cingulate gyrus in patients with AS may be related to their lack of empathy, difficulties in interacting with peers and understanding their social environment. This could also be the reason for high emotional liability and episodes of uncontrolled emotions displayed by these children.

Other abnormalities

Corpus callosum abnormalities have been reported previously in AS using MRI (Harting et al., 2009) and DTI tractography (Peters et al., 2011). The present study confirms this finding as we observed a reduced ML and SI components in corpus callosum of AS children. Involvement of the AP component of uncinate fasciculus in this study was also supported by a previous study where fractional anisotropy was reduced in uncinate fasciculus of AS children (Peters et al., 2011). They hypothesized that altered fractional anisotropy in the uncinate fasciculus which connects the amygdala to the orbito-frontal cortex may reflect impairment of social interaction observed in AS. The reduced fractional anisotropy in inferior longitudinal fasciculus/inferior fronto-occipital fasciculus tracts observed was suggested to be related to impairment in recognizing and responding to facial expressions in AS (Peters et al., 2011). The finding of decreased AP component in inferior longitudinal fasciculus region is consistent with previous observations.

Limitations

One of the limitations of this study is small sample size as AS is a rare disorder. Still, our method could potentially be used to ascertain specific nature of the abnormalities.

Conclusion

To our knowledge, this is the first study to use color-coded orientation maps to perform a TBSS procedure. The TBSS procedure performed in AS and TD children in our study showed widespread abnormalities of decreased AP, ML and SI components suggesting that the loss of UBE3A gene expression may result in widespread abnormal brain connectivity, some of which can be related to the clinical phenotype of AS. Moreover, the abnormalities in the brain regions may involve one or both the color-coded anisotropy components.

REFERENCES

Alexander DC, Pierpaoli C, Basser PJ, Gee JC. Spatial transformations of diffusion tensor magnetic resonance images. IEEE Trans Med Imaging. 2001; 20:1131–1139. [PubMed: 11700739]

Baron-Cohen, S. Precursors to a theory of mind: Understanding attention in others. Basil Blackwell; Oxford: 1991. p. 233-251.

Basser PJ, Pierpaoli C. Microstructural and physiological features of tissues elucidated by quantitative-diffusion-tensor MRI. J Magn Reson B. 1996; 111:209–219. [PubMed: 8661285]

Brun A PH, Knuttsson H Westin CF. Coloring of DT-MRI fiber traces using laplacian eigenmaps. Computer Aided Systems Theory (EUROCAST'03) LNCS. 2003; 2809:564–572. 2003.

Castro-Gago M, Gomez-Lado C, Eiris-Punal J, Rodriguez-Mugico VM. Abnormal myelination in Angelman syndrome. Eur J Paediatr Neurol. 2010; 14:292. [PubMed: 19720548]

Cheng Y, Chou KH, Chen IY, Fan YT, Decety J, Lin CP. Atypical development of white matter microstructure in adolescents with autism spectrum disorders. Neuroimage. 2010; 50:873–882. [PubMed: 20074650]

Choi J, Jeong B, Rohan ML, Polcari AM, Teicher MH. Preliminary evidence for white matter tract abnormalities in young adults exposed to parental verbal abuse. Biol Psychiatry. 2009; 65:227–234. [PubMed: 18692174]

Clayton-Smith J, Laan L. Angelman syndrome: a review of the clinical and genetic aspects. J Med Genet. 2003; 40:87–95. [PubMed: 12566516]

Dan B. Angelman syndrome: current understanding and research prospects. Epilepsia. 2009; 50:2331–2339. [PubMed: 19874386]

Dan B, Boyd SG. Angelman syndrome reviewed from a neurophysiological perspective. The UBE3A-GABRB3 hypothesis. Neuropediatrics. 2003; 34:169–176. [PubMed: 12973656]

Dan B, Servais L, Boyd SG, Wagstaff J, Cheron G. From electrophysiology to chromatin: a bottom-up approach to Angelman syndrome. Ann N Y Acad Sci. 2004; 1030:599–611. [PubMed: 15659843]

Handforth A, Delorey TM, Homanics GE, Olsen RW. Pharmacologic evidence for abnormal thalamocortical functioning in GABA receptor beta3 subunit-deficient mice, a model of Angelman syndrome. Epilepsia. 2005; 46:1860–1870. [PubMed: 16393151]

Harting I, Seitz A, Rating D, Sartor K, Zschocke J, Janssen B, Ebinger F, Wolf NI. Abnormal myelination in Angelman syndrome. Eur J Paediatr Neurol. 2009; 13:271–276. [PubMed: 18573670]

Holopainen IE, Metsahonkala EL, Kokkonen H, Parkkola RK, Manner TE, Nagren K, Korpi ER. Decreased binding of [11C]flumazenil in Angelman syndrome patients with GABA(A) receptor beta3 subunit deletions. Ann Neurol. 2001; 49:110–113. [PubMed: 11198279]

Hosford DA, Clark S, Cao Z, Wilson WA Jr. Lin FH, Morrisett RA, Huin A. The role of GABAB receptor activation in absence seizures of lethargic (lh/lh) mice. Science. 1992; 257:398–401. [PubMed: 1321503]

Hosford DA, Lin FH, Wang Y, Caddick SJ, Rees M, Parkinson NJ, Barclay J, Cox RD, Gardiner RM, Denton P, Seldin MF, Chen B. Studies of the lethargic (lh/lh) mouse model of absence seizures:

regulatory mechanisms and identification of the lh gene. Adv Neurol. 1999; 79:239–252. [PubMed: 10514818]

Jeong JW, Sundaram SK, Kumar A, Chugani DC, Chugani HT. Aberrant diffusion and geometric properties in the left arcuate fasciculus of developmentally delayed children: a diffusion tensor imaging study. AJNR Am J Neuroradiol. 2011; 32:323–330. [PubMed: 21183617]

Jiang H, van Zijl PC, Kim J, Pearlson GD, Mori S. DtiStudio: resource program for diffusion tensor computation and fiber bundle tracking. Comput Methods Programs Biomed. 2006; 81(2):106–16. [PubMed: 16413083]

Kandel A, Buzsaki G. Cellular-synaptic generation of sleep spindles, spike-and-wave discharges, and evoked thalamocortical responses in the neocortex of the rat. J Neurosci. 1997; 17:6783–6797. [PubMed: 9254689]

Koechlin E, Summerfield C. An information theoretical approach to prefrontal executive function. Trends Cogn Sci. 2007; 11:229–235. [PubMed: 17475536]

Kolb B, Milner B. Performance of complex arm and facial movements after focal brain lesions. Neuropsychologia. 1981; 19:491–503. [PubMed: 7279182]

Kuypers H. Anatomy of the descending pathways. The Nervous System, Handbook of Physiology. 1981:2.

Mayberg HS. Limbic-cortical dysregulation: a proposed model of depression. J Neuropsychiatry Clin Neurosci. 1997; 9:471–481. [PubMed: 9276848]

Peters SU, Kaufmann WE, Bacino CA, Anderson AW, Adapa P, Chu Z, Yallampalli R, Traipe E, Hunter JV, Wilde EA. Alterations in white matter pathways in Angelman syndrome. Dev Med Child Neurol. 2011; 53:361–367. [PubMed: 21121904]

Raven; et al. Raven, JC.; Court, JH.; Raven, J. Section 2: Coloured Progressive Matrices (1990 Edition, with US Norms), Manual for the Raven's Progressive Matrices and Vocabulary Scales. Oxford Psychologist Press; Oxford: 1990. 1990

Roosendaal SD, Geurts JJ, Vrenken H, Hulst HE, Cover KS, Castelijns JA, Pouwels PJ, Barkhof F. Regional DTI differences in multiple sclerosis patients. Neuroimage. 2009; 44:1397–1403. [PubMed: 19027076]

Sattler; Sattler, JM. Assessment of children. Jerome M Sattler, Publisher, Inc; San Diego: 1992. 1992

Smith SM, Jenkinson M, Johansen-Berg H, Rueckert D, Nichols TE, Mackay CE, Watkins KE, Ciccarelli O, Cader MZ, Matthews PM, Behrens TE. Tract-based spatial statistics: voxelwise analysis of multi-subject diffusion data. Neuroimage. 2006; 31:1487–1505. [PubMed: 16624579]

Sparrow, SS.; Balla, DA.; Cicchetti, DV.; Doll, EA. Vineland Adaptive Behavior Scales. American Guidance Service; Circle Pines, MN: 1984.

Stricker NH, Schweinsburg BC, Delano-Wood L, Wierenga CE, Bangen KJ, Haaland KY, Frank LR, Salmon DP, Bondi MW. Decreased white matter integrity in late-myelinating fiber pathways in Alzheimer's disease supports retrogenesis. Neuroimage. 2009; 45:10–16. [PubMed: 19100839]

Versace A, Almeida JR, Hassel S, Walsh ND, Novelli M, Klein CR, Kupfer DJ, Phillips ML. Elevated left and reduced right orbitomedial prefrontal fractional anisotropy in adults with bipolar disorder revealed by tract-based spatial statistics. Arch Gen Psychiatry. 2008; 65:1041–1052. [PubMed: 18762590]

Wechsler, D. Wechsler Preschool and Primary Scale of Intelligence. 3rd edition (WPPSI III). Psychological Corporation; San Antonio, TX: 2002.

Wechsler, D. Wechsler Intelligence Scale for Children-Fourth Edition: Administrative and scoring manual. The Psychological Corporation; San Antonio, TX: 2003.

Wilson BJ, Sundaram SK, Huq AHMM, et al. Abnormal Language Pathway in Children with Angelman Syndrome: A Diffusion Tensor Imaging (DTI) Study Annals of neurology. 2009; 66:109–109.

Wilson BJ, S.S. Huq AHMM, Chugani HT. Abnormal Language Pathway in Children with Angelman Syndrome: A Diffusion Tensor Imaging (DTI) Study. Paediatric neurology:. 2011; 44:350–356.

Xu D, Mori S, Shen D, van Zijl PC, Davatzikos C. Spatial normalization of diffusion tensor fields. Magn Reson Med. 2003; 50:175–182. [PubMed: 12815692]

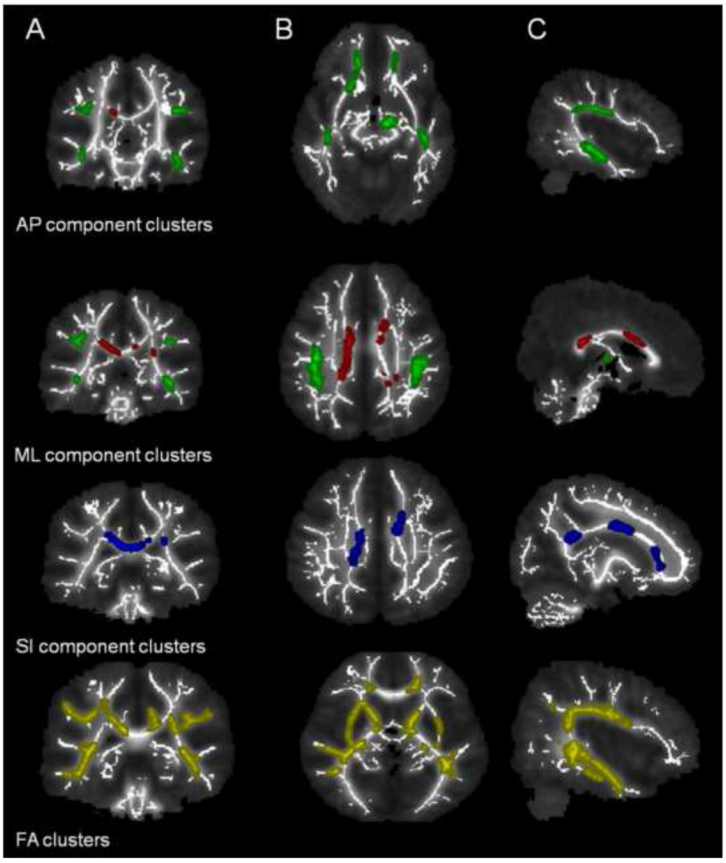

1. .

Clusters with significantly lower FA, AP, ML and SI components in AS group compared to TD group obtained after TBSS analysis. A, B and C denote the representative images of coronal, axial and saggital sections. AP component clusters (shown as green) are mainly located in arcuate fasciculus (AF), anterior thalamic radiation (ATR), cingulum, Inferior fronto-occipital fasciculus (IFO) and brainstem. ML component clusters (shown as red) are located mainly in corpus callosum, cingulum and ATR. SI components clusters (shown in blue) are located in corpus callosum and corticospinal tract. FA component clusters (shown in yellow) mostly correspond to the same locations as depicted by AP, ML and SI components.

Table 1

Mean and standard deviation of domain scores on the Vineland Adaptive Behavior Scales-II in AS group

Scale	Mean(SD)*	Adaptive Level	Mean age equivalent
Communication	56.40(11.67)	Low	1 year, 10 months
Daily Living	58.60(15.47)	Low	1 year, 3 months
Socialization	67.00(7.97)	Low	1 year, 3 months
Motor Skills	57.00(6.98)	Low	1 year, 9 months
Adaptive behavior composite	57.40(9.69)	Low	1 year, 7 months

* Scores are reported as Standard Scores (Mean=100, SD=15)

Table 2

DTI Cluster Map Analysis of AP component in Angelman Syndrome vs. Controls

		T & T Coordinates			TD	AS			
Possible tracts	**Side**	**x**	**y**	**z**	**Mean AP(s.d)**	**Mean AP(s.d)**	**% Difference**	**Voxel size**	**p value**
IFO	Left	−15	32	−8	0.33(0.03)	0.23(0.03)	33.7	3903	0.004
IFO	Right	40	−18	−14	0.37(0.02)	0.26(0.04)	34.2	1440	0.054
AF	Left	−48	−12	22	0.22(0.03)	0.10(0.02)	74.6	2450	0.006
AF	Right	35	−17	25	0.27(0.04)	0.18(0.04)	35.1	3900	0.004
ATR	Left	−20	34	−3	0.22(0.03)	0.21(0.03)	7.0	2535	0.030
ATR	Right	20	16	−12	0.34(0.02)	0.24(0.04)	34.7	5569	0.002
Cingulum	Left	−17	46	−1	0.35(0.03)	0.26(0.03)	30.1	2106	0.012
Brainstem	Right	−9	−17	−15	0.21(0.03)	0.13(0.04)	50.4	3091	0.004
Uncinate	Right	18	20	−10	0.27(0.03)	0.21(0.04)	25.1	1350	0.042

AP component = Anteroposterior component; TD = Typically developing; AS = Angelman Syndrome; IFO = Inferior fronto occipital fasciculus; AF = Arcuate fasciculus; ATR = Anterior thalamic radiation;

Table 3

DTI Cluster Map Analysis of ML component in Angelman Syndrome vs. Controls

		T & T Coordinates			TD	AS			
Possible tracts	**Side**	**x**	**y**	**z**	**Mean ML(s.d)**	**Mean ML(s.d)**	**% Difference**	**Voxel size**	**p value**
Corpus callosum	Left	7	−38	14	0.17(0.02)	0.15(0.02)	10.5	5435	0.01
Corpus callosum	Right	−10	−41	18	0.21(0.03)	0.20(0.03)	3.4	2735	0.03
ATR	Left	−10	10	23	0.09(0.03)	0.05(0.01)	51	1423	0.04
Cingulum	Right	−8	25	−4	0.27(0.11)	0.21(0.04)	24.1	1334	0.04

ML component = Mediolateral component; ATR = Anterior thalamic radiation; TD = Typically developing; AS = Angelman Syndrome

Table 4

DTI Cluster Map Analysis of SI component in Angelman Syndrome vs. Controls

		T & T Coordinates			TD	AS			
Possible tracts	**Side**	**x**	**y**	**z**	**Mean SI(s.d)**	**Mean SI(s.d)**	**% Difference**	**Voxel size**	**p value**
Corpus callosum	Left	−7	18	−5	0.33(0.03)	0.16(0.03)	68.7	5098	0.001
CST	Right	−9	−40	10	0.38(0.02)	0.20(0.02)	61.5	12389	0.0009

SI component = Su perioinfe rior component; CST = Cortic ospinal tract; TD = Typically dev eloping; AS = Angelman Syndrome

Table 5

DTI Cluster Map Analysis of Fractional anisotropy (FA) component in Angelman Syndrome vs. Controls

		T & T Coordinates			TD	AS			
Possible tracts	**Side**	**x**	**y**	**z**	**Mean FA(s.d)**	**Mean FA(s.d)**	**% Difference**	**Voxel**	**p value**
Cerebellum	Right	12	−46	−36	0.35(0.03)	0.27(0.04)	24.4	3562	0.02
Brainstem	Left	−29	−4	−31	0.38(0.03)	0.30(0.04)	26.1	5983	0.01
Cerebellum	Left	−11	−45	−30	0.34(0.03)	0.24(0.04)	32.8	2346	0.05
IFO	Right	42	−9	−25	0.38(0.02)	0.29(0.03)	27.1	4538	0.01
Brainstem	Left	−27	−8	−14	0.38(0.02)	0.31(0.03)	20.8	2890	0.01
ATR	Right	−15	33	−8	0.46(0.02)	0.36(0.04)	23.3	5678	0.01
Uncinate	Left	15	32	−8	0.45(0.03)	0.34(0.04)	28.4	3240	0.04
Cingulate	Right	−32	2	−2	0.38(0.03)	0.29(0.05)	27.4	3792	0.01
Corpus callosum	Right	9	27	8	0.49(0.02)	0.39(0.03)	23.4	2130	0.01
Corpus callosum	Left	18	47	9	0.35(0.04)	0.27(0.08)	24.6	5127	0.02
Cingulate	Right	−6	−32	22	0.41(0.03)	0.31(0.07)	29.2	2598	0.01
IFO	Right	37	−54	23	0.29(0.02)	0.21(0.08)	33.6	1423	0.01
Corpus callosum	Right	−11	−57	26	0.39(0.04)	0.33(0.06)	18.2	4567	0.01
Arcuate	Left	23	−59	33	0.43(0.02)	0.34(0.07)	23.8	5298	0.06
Cingulate	Right	33	11	40	0.35(0.02)	0.20(0.08)	25.2	3389	0.01